Available online at www.sciencedirect.com
ScienceDirect
Journal of Computational Physics 224 (2007) 941–955
JOURNAL OF COMPUTATIONAL PHYSICS
www.elsevier.com/locate/jcp

Volumetric fast multipole method for modeling Schrödinger's equation

Zhiqin Zhao [a,c], Narayan Kovvali [a], Wenbin Lin [a], Chang-Hoi Ahn [a], Luise Couchman [b], Lawrence Carin [a,*]

[a] *Department of Electrical and Computer Engineering, Duke University, Durham, NC 27708-0291, USA*
[b] *Naval Research Laboratory, Washington, DC, USA*
[c] *School of Electronic Engineering, University of Electronic Science and Technology of China, Chengdu, China*

Received 14 January 2006; received in revised form 23 October 2006; accepted 1 November 2006
Available online 22 December 2006

Abstract

A volume integral equation method is presented for solving Schrödinger's equation for three-dimensional quantum structures. The method is applicable to problems with arbitrary geometry and potential distribution, with unknowns required only in the part of the computational domain for which the potential is different from the background. Two different Green's functions are investigated based on different choices of the background medium. It is demonstrated that one of these choices is particularly advantageous in that it significantly reduces the storage and computational complexity. Solving the volume integral equation directly involves $O(N^2)$ complexity. In this paper, the volume integral equation is solved efficiently via a multi-level fast multipole method (MLFMM) implementation, requiring $O(N \log N)$ memory and computational cost. We demonstrate the effectiveness of this method for rectangular and spherical quantum wells, and the quantum harmonic oscillator, and present preliminary results of interest for multi-atom quantum phenomena.

Keywords: Volume integral method; Schrödinger's equation; Multi-level fast multipole method

1. Introduction

The efficient solution of Schrödinger's equation is an important problem in quantum nanodevice simulations. The currently available methods for solving this problem can be classified into two categories: analytical methods [1–3] and numerical methods [4–10]. Analytical methods are usually only suitable for specialized problems, with numerical methods required for most complex structures. Some of the numerical methods that have been used widely in nanodevice simulations are variational methods [4], Green's function methods [5], finite-element methods [6], finite-difference methods [7,8], and Fourier series methods [9].

* Corresponding author. Tel.: +1 919 660 5270; fax: +1 919 660 5293.
E-mail address: lcarin@ee.duke.edu (L. Carin).

0021-9991/$ - see front matter
doi:10.1016/j.jcp.2006.11.003

The pseudospectral method [10] has also been applied in quantum well simulations. Compared with the finite-difference and finite-element methods, the pseudospectral method yields solutions of higher accuracy (often, *spectral* accuracy) while requiring fewer unknowns, significantly reducing memory requirements and computational costs. However, the pseudospectral method is only suitable for problems on simple domains with smooth or regular geometry. While the method can also be applied to problems with discontinuous/singular potentials, if the spectral convergence of the numerical solution is to be retained, appropriate modifications are necessary (such as a 'multi-domain' formulation [10]). Unfortunately, this increases the complexity of the resulting scheme.

In this paper, we present a volume integral equation method for solving Schrödinger's equation for three-dimensional (3D) quantum structures. The method was first used in electromagnetic (EM) scattering problems [11–13]. An important advantage of this method is that unknowns are used only in the part of the computational domain for which the potential is different from the background. The volume integral equation method utilizes the Green's function to obtain an integral representation of Schrödinger's equation. The resulting discretization can be solved efficiently by using the fast multipole method (FMM)[1] [14–16], so that, as the problem size increases, the memory requirements and computational complexity of the method increase only as $O(N^{3/2})$ (the details of this can be found in [16,17]); by using a multi-level fast multipole method (MLFMM) [16–19], this cost scales as $O(N \log N)$.[2] In the volume integral equation method, different choices of the background medium imply use of different Green's functions. We demonstrate that careful selection of the background Green's function may significantly simplify the storage and computational complexity.

The remainder of the paper is organized as follows. In Section 2 we describe the volume integral equation method. With different choices of background, two different Green's functions are induced in the integral equation, one of which is particularly well suited for solving Schrödinger's equation. The details of FMM and MLFMM with this Green's function are discussed in Section 3. In Section 4 the method is applied to rectangular and spherical quantum wells, and the quantum harmonic oscillator, and it is also employed for a simplified investigation of multiple atoms. Conclusions are drawn in Section 5.

2. Volume integral method

The normalized time-independent 3D Schrödinger's equation may be expressed as

$$-\nabla^2\psi(\mathbf{r}) + V_{\mathrm{T}}(\mathbf{r})\psi(\mathbf{r}) = E\psi(\mathbf{r}), \quad \mathbf{r} \in \Re^3, \tag{1}$$

where $\mathbf{r}$ represents the spatial position vector, ψ denotes the wave function, V_{T} denotes the total potential, and E is the energy state. Let V_{b} represent the background potential (here assumed a constant) and let $V_{\mathrm{c}}(\mathbf{r})$ represent the potential contrast relative to V_{b}. Then

$$V_{\mathrm{T}}(\mathbf{r}) = V_{\mathrm{b}} + V_{\mathrm{c}}(\mathbf{r}), \tag{2}$$

and (1) may be rewritten as

$$\nabla^2\psi(\mathbf{r}) + [E - V_{\mathrm{b}}]\psi(\mathbf{r}) = V_{\mathrm{c}}(\mathbf{r})\psi(\mathbf{r}). \tag{3}$$

We first consider the Green's function $G_0(\mathbf{r},\mathbf{r}')$ defined via

$$\nabla^2 G_0(\mathbf{r},\mathbf{r}') + k^2 G_0(\mathbf{r},\mathbf{r}') = -\delta(\mathbf{r}-\mathbf{r}'), \tag{4}$$

where $k^2 = E - V_{\mathrm{b}}$, and we assume $V_{\mathrm{b}} < E$ in order to make k real. The Green's function is

$$G_0(\mathbf{r},\mathbf{r}') = \frac{\mathrm{e}^{-\mathrm{j}k|\mathbf{r}-\mathbf{r}'|}}{4\pi|\mathbf{r}-\mathbf{r}'|}. \tag{5}$$

This Green's function is widely applied in electromagnetic problems [12–20], and we have the solution of (3)

[1] Note that the FMM of [14] by Greengard and Rokhlin is a *multi*-level algorithm for the *static* case, and is different from the FMM discussed in this paper.

[2] For the low-frequency and static problems, it is well known that the FMM is an $O(N)$ algorithm [12,14,25,26]. The quantum problem of interest here, however, is a high-frequency dynamic case (even for the lowest energy states, the wavelength is comparable to the size of the structure), for the efficient solution of which we describe an $O(N \log N)$ MLFMM.

$$\psi(\mathbf{r}) = -\int_{\Gamma} \frac{e^{-jk|\mathbf{r}-\mathbf{r}'|}}{4\pi|\mathbf{r}-\mathbf{r}'|} V_c(\mathbf{r}')\psi(\mathbf{r}')\,d\mathbf{r}', \tag{6}$$

in which Γ represents the domain for which $V_c(\mathbf{r}) \neq 0$, i.e. the foreground. The expression in (6) represents the 'volume integral equation' form of Schrödinger's equation (3). In (4) we assumed $V_b < E$ such that k is real and the Green's function is oscillatory. In fact, we can choose V_b arbitrarily. For some problems, such as modeling quantum-atomic phenomena, the potential is everywhere negative except at the atom centers. For those cases if we choose V_b as zero, then $E - V_b < 0$. For such problems we consider an exponentially decaying Green's function $G_d(\mathbf{r},\mathbf{r}')$ satisfying

$$\nabla^2 G_d(\mathbf{r},\mathbf{r}') - k^2 G_d(\mathbf{r},\mathbf{r}') = -\delta(\mathbf{r}-\mathbf{r}'), \tag{7}$$

and the Green's function is

$$G_d(\mathbf{r},\mathbf{r}') = \frac{e^{-k|\mathbf{r}-\mathbf{r}'|}}{4\pi|\mathbf{r}-\mathbf{r}'|}. \tag{8}$$

We have the integral equation solution of Schrödinger's equation for the decaying Green's function as

$$\psi(\mathbf{r}) = -\int_{\Gamma} \frac{e^{-k|\mathbf{r}-\mathbf{r}'|}}{4\pi|\mathbf{r}-\mathbf{r}'|} V_c(\mathbf{r}')\psi(\mathbf{r}')\,d\mathbf{r}'. \tag{9}$$

Both (6) and (9) are solutions of (3), and the form that applies depends on the selected background, i.e., on whether $E - V_b$ is larger or smaller than zero. In Section 4, we show that the solution of (9) with $G_d(\mathbf{r},\mathbf{r}')$ can be performed much more efficiently than the solution of (6) with $G_0(\mathbf{r},\mathbf{r}')$. Therefore, in the following discussion, it is assumed that the form in (9) is chosen.

Using the concept employed within the method of moments (MoM) [20], we expand the wave function ψ as

$$\psi(\mathbf{r}) \approx \sum_{n=1}^{N} \alpha_n \phi_n(\mathbf{r}), \tag{10}$$

where $\phi_n(\mathbf{r})$ are the known basis functions and α_n denote the unknown expansion coefficients. Substituting this expansion into (9), we obtain

$$\sum_{n=1}^{N} \alpha_n \phi_n(\mathbf{r}) = -\sum_{n=1}^{N} \alpha_n \int_{\Gamma} \frac{e^{-k|\mathbf{r}-\mathbf{r}'|}}{4\pi|\mathbf{r}-\mathbf{r}'|} V_c(\mathbf{r}')\phi_n(\mathbf{r}')\,d\mathbf{r}'. \tag{11}$$

Converting (11) into a matrix equation via the Galerkin method, we have

$$\sum_{n=1}^{N} \alpha_n \int_{\Gamma} \phi_n(\mathbf{r})\phi_m(\mathbf{r})\,d\mathbf{r} = -\sum_{n=1}^{N} \alpha_n \int_{\Gamma} d\mathbf{r} \int_{\Gamma} \frac{e^{-k|\mathbf{r}-\mathbf{r}'|}}{4\pi|\mathbf{r}-\mathbf{r}'|} V_c(\mathbf{r}')\phi_n(\mathbf{r}')\phi_m(\mathbf{r})\,d\mathbf{r}', \tag{12}$$

which may be expressed in matrix form as

$$\mathbf{B}\boldsymbol{\alpha} = \mathbf{A}(k)\boldsymbol{\alpha}, \tag{13}$$

where the $\mathbf{A}(k)$ has elements

$$\mathbf{A}(k)_{m,n} = -\int_{\Gamma} d\mathbf{r} \int_{\Gamma} \frac{e^{-k|\mathbf{r}-\mathbf{r}'|}}{4\pi|\mathbf{r}-\mathbf{r}'|} V_c(\mathbf{r}')\phi_n(\mathbf{r}')\phi_m(\mathbf{r})\,d\mathbf{r}', \quad m,n = 1,\ldots,N, \tag{14a}$$

the matrix $\mathbf{B}$ has elements

$$\mathbf{B}_{m,n} = \int_{\Gamma} \phi_n(\mathbf{r})\phi_m(\mathbf{r})\,d\mathbf{r}, \tag{14b}$$

and $\boldsymbol{\alpha}$ is a vector comprising the unknown expansion coefficients. The expression in (13) is the volume integral discretization of the 3D Schrödinger's equation, using the integral equation form (9). The task now is to solve (13) for k and $\boldsymbol{\alpha}$, which can be done via eigenvalue shooting using a combination of Newton's method and inverse iterations [21]. Once k and $\boldsymbol{\alpha}$ have been determined, the energy states and wavefunctions are known.

The effort involved in solving the volume integral discretization (13) is as follows. If the basis functions used in the discretization procedure are sub-domain [20], then the matrix **B** is banded. For example, if a pulse basis is used, **B** is a diagonal matrix; it can then be absorbed into the vector $\boldsymbol{\alpha}$. If the structure is meshed with tetrahedrons, and scalar RWG [22] basis functions are employed, then the maximum number of non-zero elements in each row of **B** is seven. The main bottleneck is the dense matrix **A**. Directly storing this matrix requires $O(N^2)$ memory; the direct calculation of the matrix-vector products on the right-hand side of (13) is also $O(N^2)$. The fast multipole method (FMM) and multi-level fast multipole method (MLFMM) have been widely applied with the Green's function $G_0(\mathbf{r},\mathbf{r}')$ to decrease the memory and computational requirements for solving such integral equations [12–19]. Both the memory and the computational cost for FMM are of $O(N^{1.5})$, and they are $O(N\log N)$ for MLFMM.

The exponentially decaying Green's function $G_d(\mathbf{r},\mathbf{r}')$ has important advantages over the Green's function $G_0(\mathbf{r},\mathbf{r}')$ used widely in electromagnetics. First, while $G_0(\mathbf{r},\mathbf{r}')$ is complex, $G_d(\mathbf{r},\mathbf{r}')$ is real, and therefore the memory required when using $G_d(\mathbf{r},\mathbf{r}')$ is only half the memory needed for $G_0(\mathbf{r},\mathbf{r}')$. Moreover, computations are often much faster with real numbers than with complex numbers. Therefore, using $G_d(\mathbf{r},\mathbf{r}')$ yields significant savings in both memory and computation. In addition, since $G_d(\mathbf{r},\mathbf{r}')$ is exponentially decaying the interaction matrix is strictly diagonally dominant, which as demonstrated below greatly improves the convergence rate of the iterative solver for (13).

3. FMM and MLFMM for the volume integral method with the decaying Green's function G_d

In this section, we turn to the FMM and MLFMM for the volume integral method with the decaying Green's function G_d. To our knowledge this work represents the first time FMM/MLFMM have been applied with G_d, so details are provided. We discuss, in particular, the advantages afforded when G_d is used as opposed to G_0.

Two identities constitute the foundation of FMM. The first is the expansion of the Green's function using Gegenbauer's addition theorem

$$G_d(\mathbf{r},\mathbf{r}') = \frac{e^{-kR}}{4\pi R} = \frac{e^{-k|\mathbf{D}+\mathbf{d}|}}{4\pi|\mathbf{D}+\mathbf{d}|} = -\frac{k}{4\pi}\sum_{l=0}^{\infty}(-1)^l(2l+1)j_l(jkd)h_l^{(1)}(jkD)P_l(\hat{\mathbf{d}}\cdot\hat{\mathbf{D}}), \tag{15}$$

where $j_l(\,)$ is the first kind spherical Bessel function, $h_l^{(1)}(\,)$ is the first kind spherical Hankel function, and $P_l(\,)$ is the Legendre polynomial. As shown in Fig. 1, $R = |\mathbf{r}-\mathbf{r}'| = |\mathbf{D}+\mathbf{d}|$, $\mathbf{r}$ and $\mathbf{r}'$ are the observation and source points, $\mathbf{r}_m$ and $\mathbf{r}'_m$ are the corresponding group centers, $\mathbf{D} = \mathbf{r}_m - \mathbf{r}'_m$ is a vector between the two group centers, $\mathbf{d} = (\mathbf{r}'_m - \mathbf{r}') + (\mathbf{r} - \mathbf{r}_m)$ and $d < D$.

The second identity used in the FMM is the expansion of $j_l(jkd)P_l(\hat{\mathbf{d}}\cdot\hat{\mathbf{D}})$ as an integration of propagating plane waves:

$$j_l(jkd)P_l(\hat{\mathbf{d}}\cdot\hat{\mathbf{D}}) = \frac{1}{4\pi i^l}\int e^{-\mathbf{k}\cdot\mathbf{d}}P_l(\hat{\mathbf{k}}\cdot\hat{\mathbf{D}})\,d^2\hat{\mathbf{k}}, \tag{16}$$

where $\hat{\mathbf{k}}$ are unit vectors on a unit sphere. Substitution of (16) into (15) yields

$$G_d(\mathbf{r},\mathbf{r}') = \frac{-k}{(4\pi)^2}\int d^2\hat{\mathbf{k}}e^{-\mathbf{k}\cdot\mathbf{d}}\sum_{l=0}^{\infty}(i)^l(2l+1)h_l^{(1)}(jkD)P_l(\hat{\mathbf{k}}\cdot\hat{\mathbf{D}}). \tag{17}$$

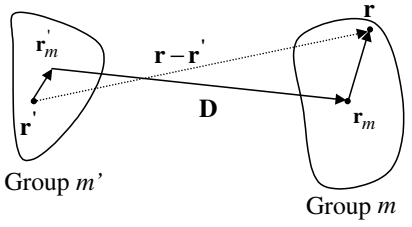

Fig. 1. Geometrical relationships between the source and observation points.

The summation on the right-hand side of (17) is a function of kD and $\hat{\mathbf{k}} \cdot \hat{\mathbf{D}}$. It is denoted by the translation operator

$$T(kD, \hat{\mathbf{k}} \cdot \hat{\mathbf{D}}) = \sum_{l=0}^{\infty} (i)^l (2l+1) h_l^{(1)}(jkD) P_l(\hat{\mathbf{k}} \cdot \hat{\mathbf{D}}). \tag{18}$$

In numerical computation the series in (18) must be truncated. Let $T_L(\,)$ denote the truncated series with the first $L+1$ terms, we have

$$T_L(kD, \hat{\mathbf{k}} \cdot \hat{\mathbf{D}}) = \sum_{l=0}^{L} (i)^l (2l+1) h_l^{(1)}(jkD) P_l(\hat{\mathbf{k}} \cdot \hat{\mathbf{D}}). \tag{19}$$

The benefit of FMM is that the translation operators $T_L(\,)$ between groups can be pre-computed before the iterative solution, and the interactions between the elements in the two groups can be computed once through the translation operator [16,17].

The error in the truncated Green's function is

$$\varepsilon = \left| \sum_{l=L+1}^{\infty} (-1)^l (2l+1) j_l(jkd) h_l^{(1)}(jkD) P_l(\hat{\mathbf{d}} \cdot \hat{\mathbf{D}}) \right| \tag{20}$$

and the error is maximum when $\mathbf{D}$ and $\mathbf{d}$ are collinear [24]. Applying the large argument approximation of the spherical Hankel function, the error can be approximated as

$$\varepsilon \approx \frac{e^{-kD}}{D} \left| \sum_{l=L+1}^{\infty} i^l (2l+1) j_l(jkd) \right| \leqslant \frac{e^{-kD}}{D} (2L+3) |j_{L+1}(jkd)| \leqslant \frac{e^{-kD}}{D} (2L+3) j_{L+1}(kd). \tag{21}$$

Compared with the error given in (3.41) of [12] for the oscillatory Green's function $G_0(\mathbf{r}, \mathbf{r}')$, the error of the decaying Green's function $G_d(\mathbf{r}, \mathbf{r}')$ has an extra factor e^{-kD}. For the problems of interest here, kD is often much larger than one, and the expansion using the Green's function $G_d(\mathbf{r}, \mathbf{r}')$ has much smaller error than using $G_0(\mathbf{r}, \mathbf{r}')$. Fig. 2 shows the comparison of the errors in the translation operator using different Green's functions for different L.

Following the same derivation as in Chew et al. [12], the relationship between L and the error ε may be expressed as

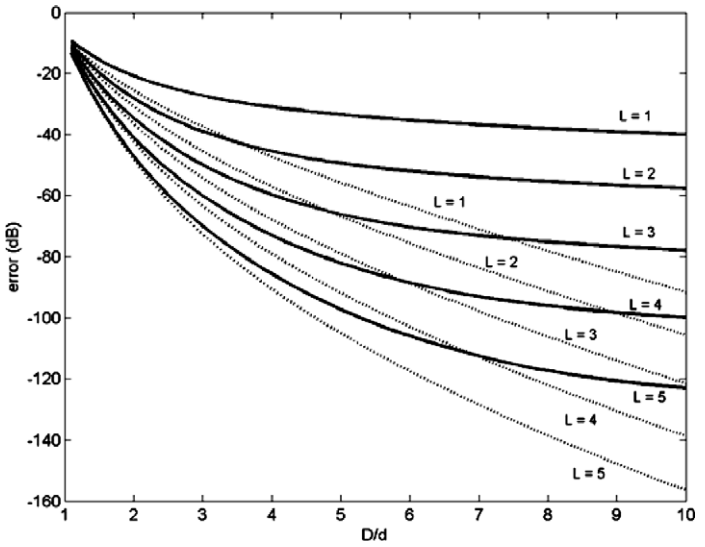

Fig. 2. Comparison of the errors in the translation operator using different Green's functions for different L. The solid lines and dotted lines are for $G_0(\mathbf{r}, \mathbf{r}')$ and $G_d(\mathbf{r}, \mathbf{r}')$, respectively. In this figure d is fixed at 0.1 and k is fixed at 2π.

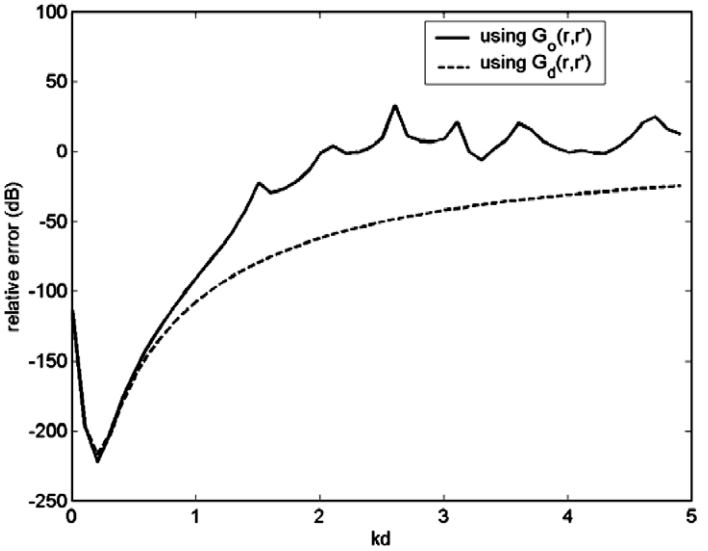

Fig. 3. Comparison of the errors in the plane wave expansion using different Green's functions.

$$L \approx kd + 1.8d_0^{2/3}(kd)^{2/3}, \tag{22}$$

where $d_0 = \log\left(\frac{e^{-kD}}{D}\cdot\frac{1}{\varepsilon}\right)$. In (22), L can be negative when kD is very large, implying that we can just neglect the interaction between these two groups because $G_d(\mathbf{r},\mathbf{r}')$ is exponential decaying.

In the implementation of the plane wave expansion (16), a Gauss–Legendre quadrature [16] is applied. The error induced by this approximation for the decaying Green's function $G_d(\mathbf{r},\mathbf{r}')$ is almost always less than that for the oscillatory Green's function $G_0(\mathbf{r},\mathbf{r}')$. Fig. 3 is a sample for the same number of discrete $\hat{\mathbf{k}}$. The Green's function $G_d(\mathbf{r},\mathbf{r}')$ has less relative error for large kd. In this case, the number of $\hat{\mathbf{k}}$ used is 200, and the order of the first kind spherical Bessel function is five. The expansion using $G_d(\mathbf{r},\mathbf{r}')$ is generally more accurate, but around the null they are similar. Therefore, we still use the same criterion to set the number of plane waves as that of $G_0(\mathbf{r},\mathbf{r}')$ [16] in order to guarantee solution accuracy.

Using the expansion as described above, the interaction matrix (14a) can be rewritten as

$$\mathbf{A}(k)_{n,n'} \approx \frac{k}{(4\pi)^2}\int_\Gamma \mathrm{d}\mathbf{r}\phi_n(\mathbf{r})\int_\Gamma \phi_{n'}(\mathbf{r}')V_c(\mathbf{r}')\,\mathrm{d}\mathbf{r}'\int \mathrm{d}^2\hat{\mathbf{k}}e^{-\mathbf{k}\cdot\mathbf{d}}T_L(kD,\hat{\mathbf{k}}\cdot\hat{\mathbf{D}}). \tag{23}$$

Let $\mathbf{r}_{m'}$ be the center of the group containing the source element n', $\mathbf{r}_m$ be the center of the group center containing the observation element n, $\mathbf{d} = (\mathbf{r}_{m'} - \mathbf{r}') + (\mathbf{r} - \mathbf{r}_m)$, and $\mathbf{D} = \mathbf{r}_m - \mathbf{r}_{m'}$. The expression in (23) may now be rewritten as

$$\mathbf{A}(k)_{n,n'} \approx \frac{k}{(4\pi)^2}\int \mathrm{d}^2\hat{\mathbf{k}}\int_\Gamma \mathrm{d}\mathbf{r}e^{-\mathbf{k}\cdot(\mathbf{r}-\mathbf{r}_m)}\phi_n(\mathbf{r})\int_\Gamma e^{\mathbf{k}\cdot(\mathbf{r}'-\mathbf{r}_{m'})}\phi_{n'}(\mathbf{r}')V_c(\mathbf{r}')\,\mathrm{d}\mathbf{r}'T_L(kD,\hat{\mathbf{k}}\cdot\hat{\mathbf{D}}). \tag{24}$$

The remaining details of the implementation of FMM and MLFMM with G_d are *identical* to those of the G_0 case. For brevity, we do not include them here but rather refer the reader to the literature [12–19].

4. Simulation results

The advantages of the volume integral equation method using the exponentially decaying Green's function are demonstrated through simulation of a 3D rectangular quantum well, a 3D spherical quantum well, and a 3D quantum harmonic oscillator. The agreement between the numerical and the analytical solutions is shown. For the harmonic oscillator problem, we compare the solution from the volume integral equation method with that from the pseudospectral method using Chebyshev polynomials as basis functions [27]. Finally, the method is applied to a problem of interest for multi-atom quantum problems. Because we used the normalized

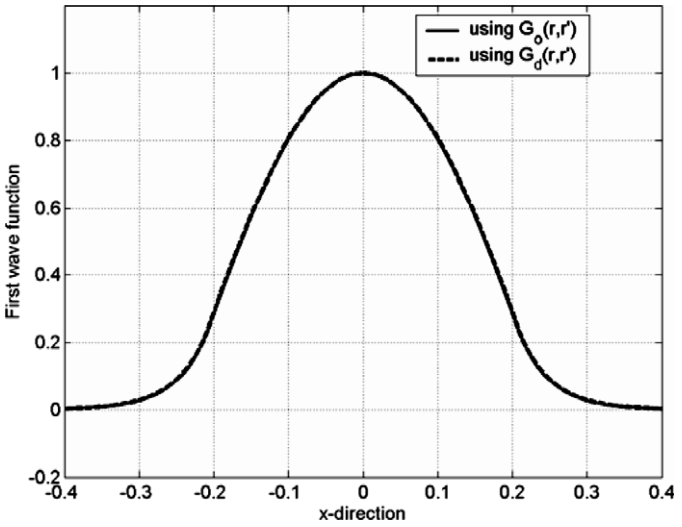

Fig. 4. First wave function in the x-direction obtained from the volume integral method for the 3D rectangular quantum well problem, for two different Green's functions: $G_0(\mathbf{r},\mathbf{r}')$ and $G_d(\mathbf{r},\mathbf{r}')$. When using $G_0(\mathbf{r},\mathbf{r}')$, the outside region is meshed with 4250 unknowns, and when using $G_d(\mathbf{r},\mathbf{r}')$, the inside region is meshed with only 250 unknowns.

time-independent 3D Schrödinger's equation in (1), the parameters in the following simulations are dimensionless.

4.1. Rectangular quantum well

For the rectangular quantum well, the potential function is

$$V(x,y,z)=\begin{cases}200\pi, & \text{outside the cube } [-0.2,0.2]\times[-0.1,0.1]\times[-0.1,0.1],\\ 0, & \text{otherwise,}\end{cases}\quad \text{for } (x,y,z)\in\Re^3. \tag{25}$$

The background potential may be chosen as $V_b=0$, so that unknowns are only needed *outside* the well, and the infinite outside region is regarded as foreground and therefore must be truncated. The domain is truncated to the cube $[-0.4,0.4]\times[-0.3,0.3]\times[-0.3,0.3]$ and uniformly meshed with 4250 small cubes. Because $E-V_b>0$, the oscillatory Green's function $G_0(\mathbf{r},\mathbf{r}')$ is used here. The solid line in Fig. 4 shows the first wave function in the x direction for this rectangular quantum well.

Alternatively, we may choose $V_b=200\pi$, so that the nonzero region is only inside the well. Therefore, we only need to mesh the *inside* of the well, and no domain truncation is required. Because $E-V_b<0$, the decaying Green's function $G_d(\mathbf{r},\mathbf{r}')$ is used. With this choice, since the region inside the well is relatively small, the number of unknowns required is small; 250 small cubes are meshed inside the well with the same step size as that for meshing the outside. The dashed line in Fig. 4 is the result of the first wave function using $G_d(\mathbf{r},\mathbf{r}')$. The results using $G_0(\mathbf{r},\mathbf{r}')$ and $G_d(\mathbf{r},\mathbf{r}')$ agree with each other well. The relative difference is 0.3%, which is defined as

$$\varepsilon=\left[\frac{\int\int\int[\psi_0(x,y,z)-\psi_d(x,y,z)]^2\,dx\,dy\,dz}{\int\int\int\psi_0^2(x,y,z)\,dx\,dy\,dz}\right]^{1/2}, \tag{26}$$

where $\psi_0(x,y,z)$ and $\psi_d(x,y,z)$ are the wave functions computed by using $G_0(\mathbf{r},\mathbf{r}')$ and $G_d(\mathbf{r},\mathbf{r}')$, respectively.

Using the decaying Green's function $G_d(\mathbf{r},\mathbf{r}')$ has important advantages, especially when the foreground is small compared with the background. In addition to the advantages in memory requirement and CPU-time, it needs much less unknowns for this case: 250 unknowns vs. 4250 unknowns when using $G_0(\mathbf{r},\mathbf{r}')$. This, coupled with the accelerated convergence of the GMRES iterative solver [23], greatly improves the performance of the method.

In order to compare the convergence speed of the GMRES iterative solver, a similar numbers of unknowns are used for the different Green's functions. Fig. 5 shows a comparison on the convergence speed using

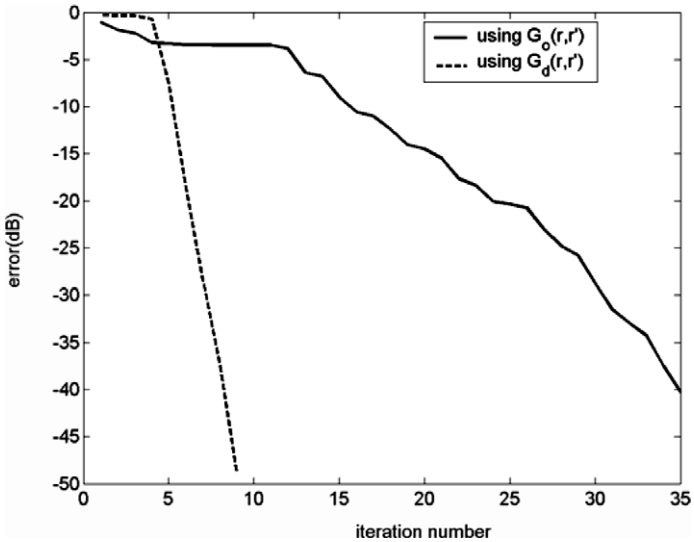

Fig. 5. Comparison of the convergence of GMRES iterations using different Green's functions $G_0(\mathbf{r},\mathbf{r}')$ and $G_d(\mathbf{r},\mathbf{r}')$. When using $G_0(\mathbf{r},\mathbf{r}')$, the outside region of quantum well is meshed with 2125 unknowns, and when using $G_d(\mathbf{r},\mathbf{r}')$, the inside region is meshed with 2000 unknowns.

different Green's functions for the first mode of the same quantum problem described in (25). When using $G_0(\mathbf{r},\mathbf{r}')$ we mesh the outside region with 2125 unknowns, and when using $G_d(\mathbf{r},\mathbf{r}')$ we mesh the inside region with 2000 unknowns. The two unknown numbers are somewhat different, but this does not affect the comparison significantly. The convergence speed is much faster when using $G_d(\mathbf{r},\mathbf{r}')$ due to the well-conditioned properties of the associated matrix equation.

The above results were obtained using MoM, whose memory requirement and computational cost grows as $O(N^2)$. Since the new Green's function $G_d(\mathbf{r},\mathbf{r}')$ has important advantages over $G_0(\mathbf{r},\mathbf{r}')$, all of the following results (unless explicitly stated otherwise) are computed using $G_d(\mathbf{r},\mathbf{r}')$.

The volume integral method is next implemented using MLFMM, and a comparison between MoM and MLFMM shown in Fig. 6. The inner region of the well is meshed uniformly with 2000 cubes. The MLFMM

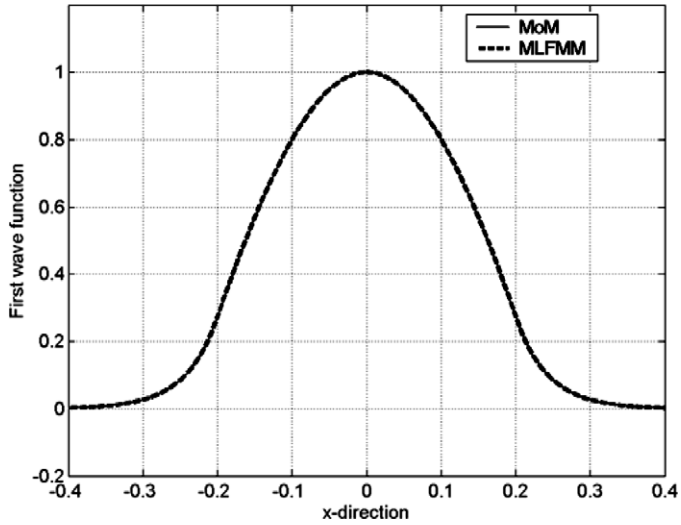

Fig. 6. Comparison of the first wave function of the rectangular quantum well using MoM and MLFMM. The inner region of the well is meshed uniformly with 2000 cubes.

result agrees very well with that of MoM – the relative mean square error (MSE) for MLFMM is 0.06% with reference to MoM results.

The total memory required and computational cost (per GMRES iteration) of the MLFMM result is much less than direct multiplication, as shown in Figs. 7 and 8, where the problem size is increased keeping the sampling density fixed, so that the number of unknowns N increases. The costs of the direct solver (MoM) scale as $O(N^2)$, where as the costs of the MLFMM increase as $O(N \log N)$, which, for the ranges of unknowns

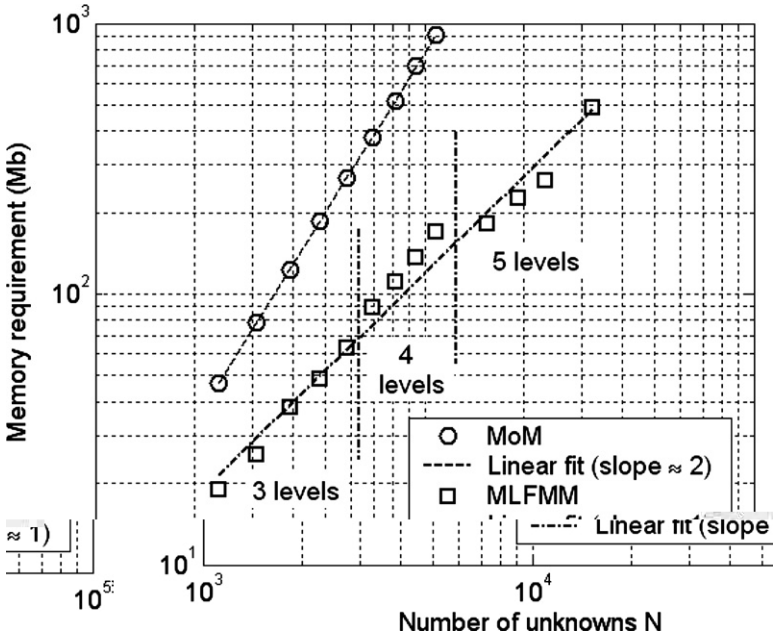

Fig. 7. Memory required in the MoM and MLFMM volume integral solutions of the 3D rectangular quantum well problem. The number of MLFMM levels is indicated as a function of N.

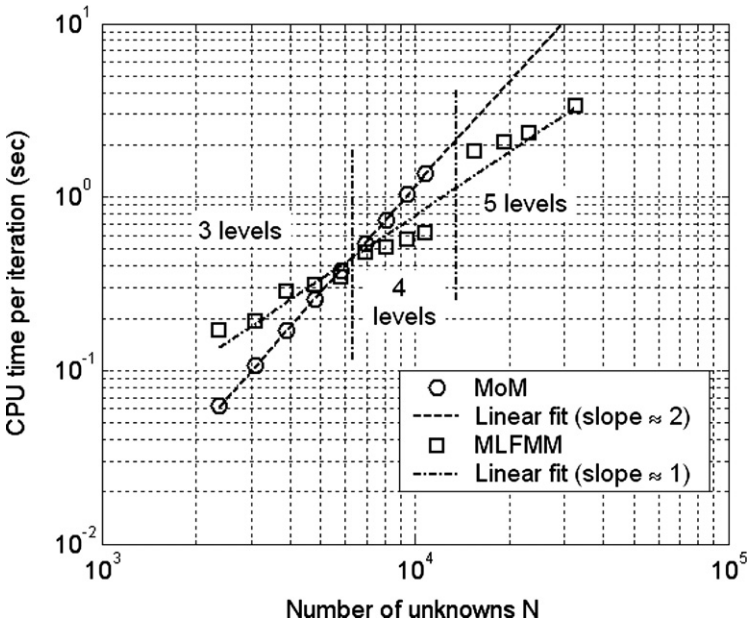

Fig. 8. Computational cost for the MoM and MLFMM volume integral solutions of the 3D rectangular quantum well problem.

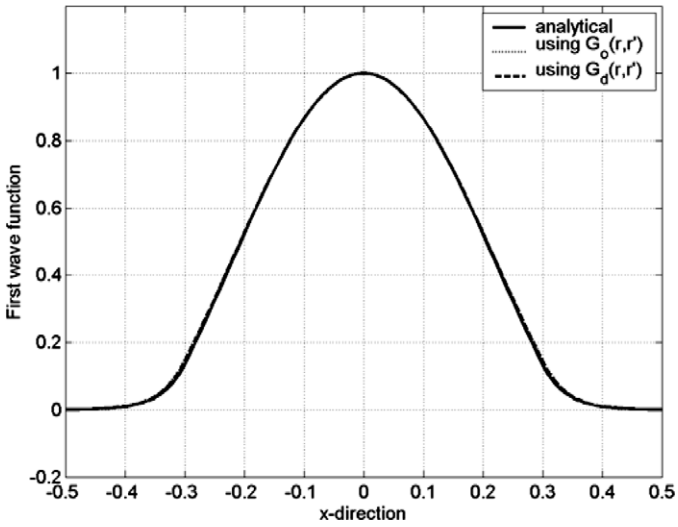

Fig. 9. First wave function in the x-direction obtained from the volume integral method for the 3D spherical quantum well problem using different Green's functions. When using $G_0(\mathbf{r},\mathbf{r}')$, the domain $0.3 \leqslant r \leqslant 0.5$ is meshed with 3312 unknowns, and when using $G_d(\mathbf{r},\mathbf{r}')$, the domain $r \leqslant 0.3$ is meshed with 4224 unknowns.

considered here, is almost only a linear rate of increase. In Figs. 7 and 8, the curves of MLFMM are not exactly linear; this is because different levels are used, as shown in the figures. Overall, MLFMM is implemented with a cost on the order of $O(N \log N)$.

4.2. Spherical quantum well

We now consider a spherical quantum well with potential

$$V(x,y,z) = \begin{cases} 200\pi, & \sqrt{x^2+y^2+z^2} > 0.3 \\ 0, & \text{otherwise,} \end{cases} \quad \text{for } (x,y,z) \in \Re^3. \tag{27}$$

In the volume integral solution of this problem, we first choose the background potential as $V_b = 0$, so that unknowns are needed only outside the well (because V_c is non-zero only in that region), and the Green's function $G_0(\mathbf{r},\mathbf{r}')$ is used. The domain is truncated to a sphere with radius $r = 0.5$. The domain $0.3 \leqslant r \leqslant 0.5$ is meshed with 3312 small cubes. The dotted lines of Figs. 9 and 10 are the first and second symmetric wave functions along the x-direction using $G_0(\mathbf{r},\mathbf{r}')$. Compared with the analytical results which are shown as a solid line in Figs. 9 and 10, the relative mean-square-error (MSE) of the wave functions are about -40.4 and -35.7 dB for both modes, respectively.

We now choose the background potential as $V_b = 200\pi$, with unknowns needed only inside the well. As $E - V_b < 0$, we use the decaying Green's function $G_d(\mathbf{r},\mathbf{r}')$. The dashed lines in Figs. 9 and 10 show the first and second symmetric wave functions in x-direction of this spherical quantum well with $G_d(\mathbf{r},\mathbf{r}')$, respectively, using $N = 4224$ unknowns. The relative MSE in the wave functions are about -42 and -37 dB for both modes, respectively (with the analytical solution as reference).

The convergence speeds using the different Green's functions for the first mode of this spherical quantum problem are compared in Fig. 11. We observe that the convergence speed is much faster when using $G_d(\mathbf{r},\mathbf{r}')$, due to the well-conditioned properties of the associated matrix equation.

In order to avoid the errors brought by MLFMM expansions, the above comparisons were obtained using MoM. In our test, the MLFMM using oscillatory Green's function $G_0(\mathbf{r},\mathbf{r}')$ was not accurate for computation of the eigen states. This is because the interactions between the well-separated elements are still relatively large and the contributions from these elements may cancel the contribution from the contributions from near elements, therefore very accurate expansions are needed in the MLFMM. By comparison the MLFMM with $G_d(\mathbf{r},\mathbf{r}')$ was found to perform with high accuracy; this is because the interactions between the well-separated

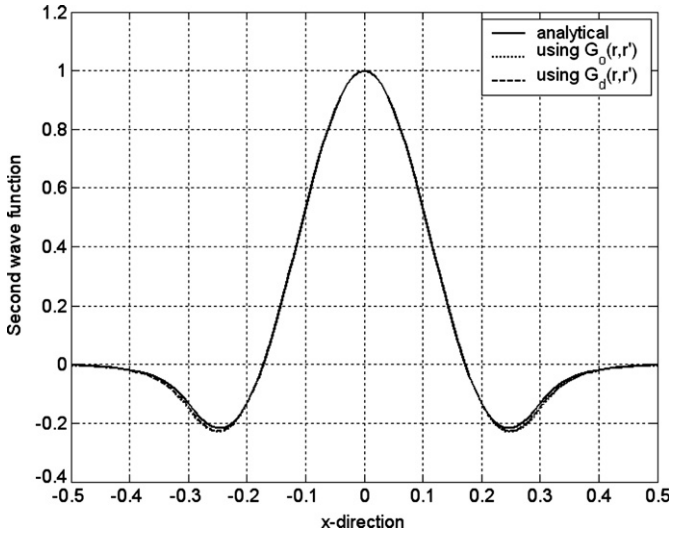

Fig. 10. Second wave function in the x-direction obtained from the volume integral method for the 3D spherical quantum well problem using different Green's functions. When using $G_0(\mathbf{r},\mathbf{r}')$, the domain $0.3 \leqslant r \leqslant 0.5$ is meshed with 3312 unknowns, and when using $G_d(\mathbf{r},\mathbf{r}')$, the domain $r \leqslant 0.3$ is meshed with 4224 unknowns.

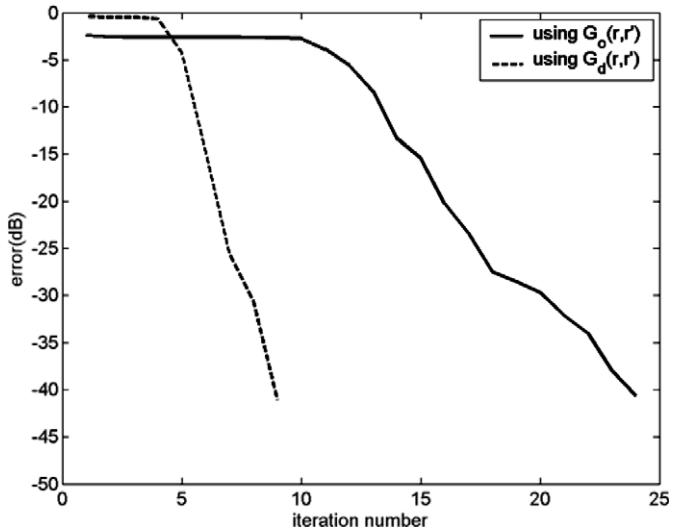

Fig. 11. Comparison of the convergence of GMRES iterations using Green's function $G_0(\mathbf{r},\mathbf{r}')$ and $G_d(\mathbf{r},\mathbf{r}')$. When using $G_0(\mathbf{r},\mathbf{r}')$, the domain $0.3 \leqslant r \leqslant 0.5$ of the spherical quantum well is meshed with 3312 unknowns, and when using $G_d(\mathbf{r},\mathbf{r}')$, the domain $r \leqslant 0.3$ is meshed with 4224 unknowns.

elements are very small compared to the near-interaction terms. The MLFMM result using $G_d(\mathbf{r},\mathbf{r}')$ and the MoM result are almost identical and therefore not shown here.

4.3. Comparison with the Chebyshev pseudospectral method for the 3D quantum harmonic oscillator

For the quantum harmonic oscillator, the potential function is

$$V(x,y,z) = x^2 + y^2 + z^2 \quad \text{for } (x,y,z) \in \Re^3. \tag{28}$$

The analytical solution of this problem is well known, and the energy states are

$$E^{\mathrm{an}}_{n_x,n_y,n_z} = (2n_x + 1) + (2n_y + 1) + (2n_z + 1), \tag{29}$$

for $n_x, n_y, n_z = 0, 1, \ldots$, with the corresponding separable wave functions give by

$$\psi^{\mathrm{an}}_{n_x,n_y,n_z}(x, y, z) = \exp\left[-\frac{x^2}{2}\right] H_{n_x}(x) \exp\left[-\frac{y^2}{2}\right] H_{n_y}(y) \exp\left[-\frac{z^2}{2}\right] H_{n_z}(z), \tag{30}$$

where H_n denotes the Hermite polynomial of order n.

In both the volume integral equation method and the Chebyshev pseudospectral method, the domain was truncated to the cube $[-8,8]\times[-8,8]\times[-8,8]$. In the volume integral method, simple pulse basis functions were employed and the background was chosen as $V_b = 0$. Therefore, $E_\lambda - V_b > 0$, and the Green's function $G_0(\mathbf{r}, \mathbf{r}')$ is used.

Fig. 12 plots the first wave function in the x-direction obtained from the Chebyshev pseudospectral and volume integral methods, both using 4096 unknowns. For comparison, the analytical solution has also been included in the same figure. We can see that the solution from the volume integral equation method agrees very well with the analytical solution. The solution from the Chebyshev pseudospectral method, on the other hand, is not as good. The main reason for this is twofold. Firstly, the Chebyshev pseudospectral method utilizes a non-uniform gird with the density of the collocation positions being very low in the center of the domain; but this is where the wave function primarily resides. This low resolution near the domain center limits the accuracy of the Chebyshev pseudospectral method, whereas the volume integral equation method utilizes a uniform grid and does not suffer from this problem. Secondly, the Chebyshev pseudospectral method *wastes* unknowns, in that it unnecessarily uses too many grid points near the domain boundaries where the wave function is nearly zero.

Fig. 13 shows the comparison of the first wave function in the x-direction obtained from the Chebyshev pseudospectral and volume integral method using 8000 unknowns, with the analytical wave function. We can see that the accuracy of the Chebyshev pseudospectral solution has improved significantly. But now the solution from the volume integral method is almost indistinguishable from the analytic solution.

Fig. 14 shows the relative error in the first energy state obtained from the Chebyshev pseudospectral and volume integral method, as a function of unknown number. We can see that both the methods yield spectrally accurate solutions. For any given number of unknowns, the solution from the volume integral method is clearly more accurate than that from the Chebyshev pseudospectral method.

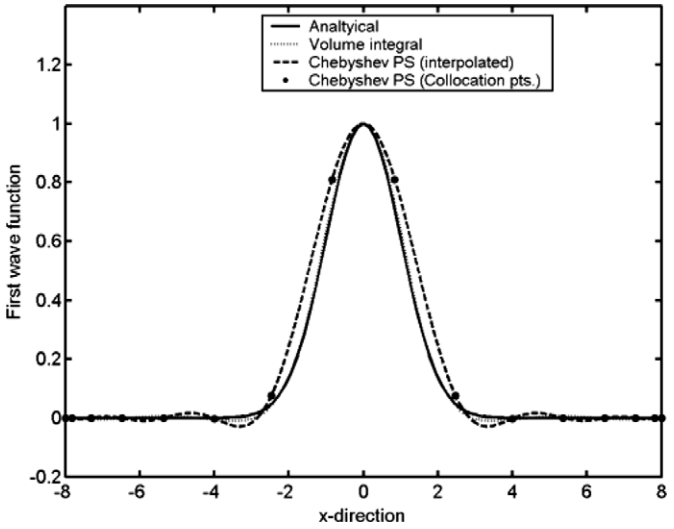

Fig. 12. First wave function in the x-direction obtained from the Chebyshev pseudospectral and volume integral equation method for the 3D quantum harmonic oscillator problem, using 4096 unknowns.

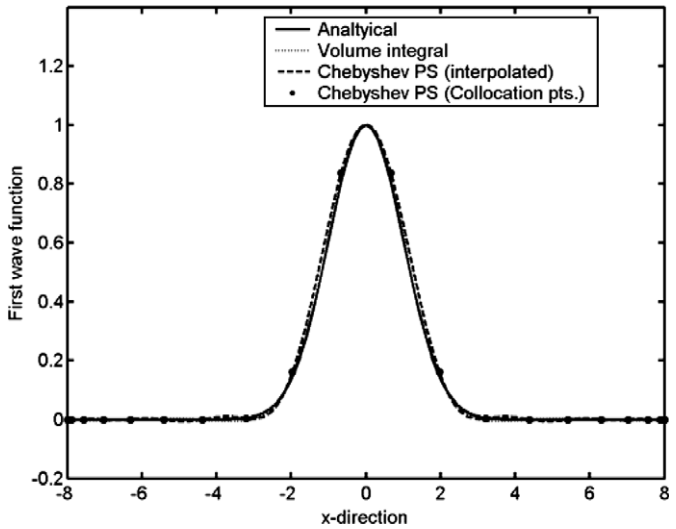

Fig. 13. First wave function in the x-direction obtained from the Chebyshev pseudospectral and volume integral equation method for the 3D quantum harmonic oscillator problem, using 8000 unknowns.

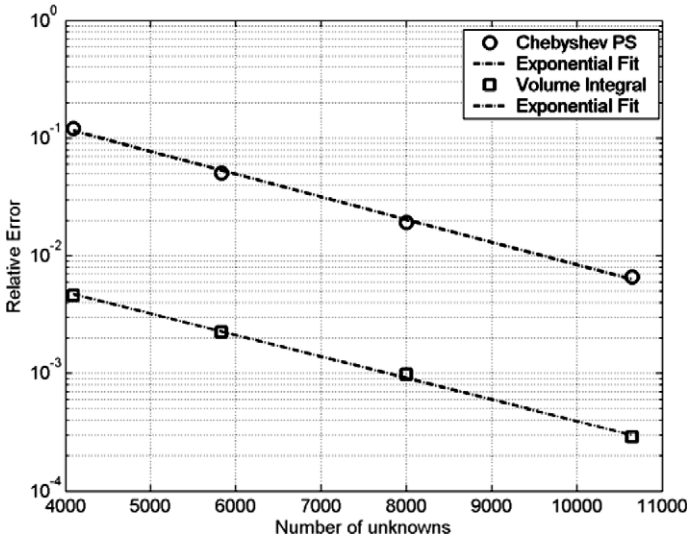

Fig. 14. Relative error in the first energy state of the 3D quantum harmonic oscillator problem obtained from the Chebyshev pseudospectral and volume integral equation method with MLFMM, as a function of unknown number.

4.4. Multi-atom case

The volume integral equation method is now used to investigate a simple rendering of a multi-atom quantum problem. The simulation domain is $[0, 8.5] \times [0, 6.25] \times [0, 6.25]$ bohr. The centers of two carbon atoms are kept at $(3.125, 3.125, 3.125)$ and $(5.375, 3.125, 3.125)$ bohr and the bond length of these two atoms is 2.25 bohr (about 1.2 Å). The domain is uniformly meshed with 21,250 cubes. Because the potential of a single atom is $-\frac{Z_a}{r}$ (Z_a is the valence), for the first several modes $E_\lambda - V_b < 0$ is always valid. Hence, the integral method using the decaying Green's function $G_d(\mathbf{r}, \mathbf{r}')$ with a 4-level MLFMM is applied to simulate this case. This simulation was run on 3.06 GHz Intel Xeon processor. The total RAM required is 273 Mbytes. In the solution of the eigen problem, it takes three inverse iterations to achieve 10^{-3} relative error. In each inverse iteration, the GMRES linear solver requires about 12 iterations to converge to 10^{-2}. For each GMRES iteration 1.6 s are required.

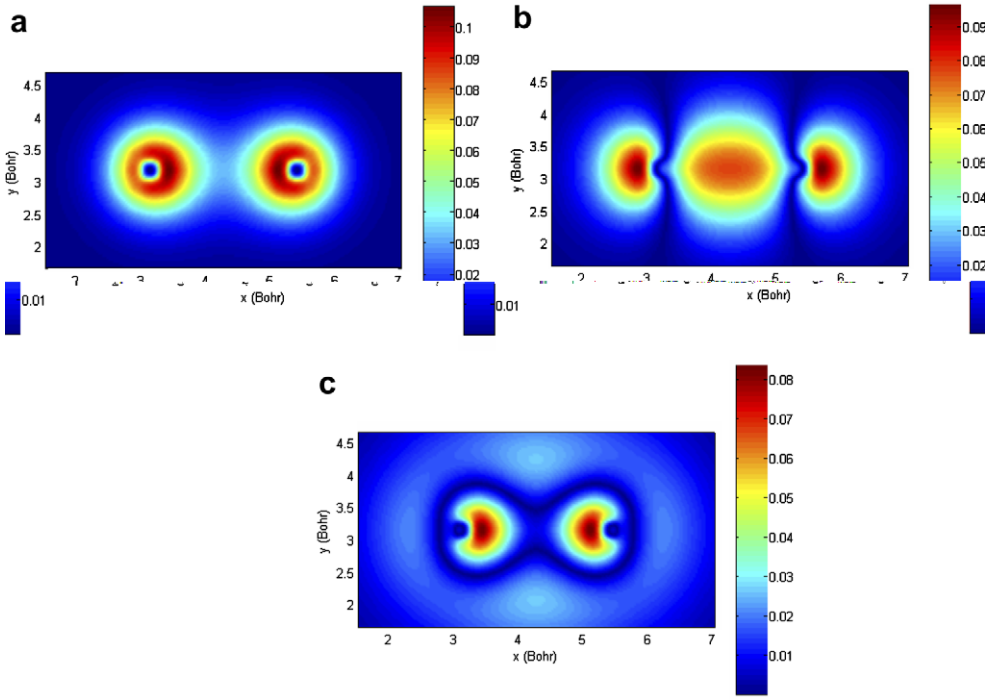

Fig. 15. Wave functions obtained using volume integral equation method for a simple rendering of two carbon atoms. The simulation domain is uniformly meshed with 21,250 cubes. (a) The first wave function; (b) the second wave function; (c) the third wave function.

Fig. 15a shows the first wave functions (in the xy plane at $z = 0$). The results show that the electrons are more likely to orbit around their own atom centers. Fig. 15b is the second wave function; a covalence is clearly formed between the two atoms. Fig. 15c is the third wave function; a common orbital around these two atoms is formed. All results show that the volume integral equation method using the decaying Green's function can be further applied to atomic simulations (with a more-realistic handling of the potential). Further studies are undergoing in this direction.

5. Conclusion

A volume integral equation method has been developed for solving Schrödinger's equation for 3D quantum structures. The method is very flexible for problems with arbitrary geometry and potential distribution, and has the important advantage of requiring unknowns only in the part of the computational domain where the potential is different from the background. For problems in which the background potential occupies a relatively large portion of the domain, the savings in the number of unknowns used are significant. Different choices of background potential induce different Green's functions. One of these, an exponentially decaying Green's function, is shown to have important advantages over the conventional oscillatory one. As the problem size increases, both the memory requirement and computational complexity of the volume integral equation method (using MLFMM) scale as $O(N \log N)$. In our numerical simulation results, the volume integral equation method shows very accurate solutions.

For a given quantum problem, by suitable choice of the 'background' potential V_b, the integral-equation can be formulated for solution using either the oscillatory Green's function G_0 (conventional) or the exponentially decaying Green's function G_d (new). Our experiments clearly indicate that the formulation involving G_d has definitive advantages over that of G_0. Also, the Green's functions G_0 and G_d depend on the potential function $V(x, y, z)$ (through k and V_b).

As discussed in Section 1, most electromagnetic simulations performed with volume integral equations utilize the oscillatory Green's function G_0. There are, however, problems in electromagnetics that would profit

from use of the decaying Green's function G_d utilized here. Specifically, there is a dual between the eigenmodes of a quantum structure and the eigenmodes of a dielectric waveguide [20]. For such problems utilization of G_d may provide computational advantages vis-à-vis G_0, and as demonstrated here the MLFMM may be utilized to further advance computational efficiency.

Acknowledgments

The authors thank the anonymous reviewers whose valuable comments and suggestions substantially improved the presentation, both in form and content.

References

[1] E.J. Austin, M. Jaros, Electronic structure of an isolated GaAs–GaAlAs quantum well in a strong electric field, Phys. Rev. B 31 (1985) 5569.
[2] D.A.B. Miller, D.S. Chemla, T.C. Damen, A.C. Gossard, W. Wiegmann, T.H. Wood, C.A. Burrus, Electric field dependence of optical absorption near the band gap of quantum-well structures, Phys. Rev. B 32 (1985) 1043.
[3] S. Panda, B.K. Panda, Analytic methods for field induced tunneling in quantum wells with arbitrary potential profiles, Pramana, J. Phys. 56 (2001) 809.
[4] G. Bastard, E.E. Mendez, L.L. Chang, L. Esaki, Variational calculations on a quantum well in an electric field, Phys. Rev. B 28 (1983) 3241.
[5] S.L. Chuang, S. Schimitt-Rink, D.A. Miller, D.S. Chemla, Exciton Green's-function approach to optical absorption in a quantum well with an applied electric field, Phys. Rev. B 43 (1991) 1500.
[6] K. Nakamura, A. Shimizu, M. Koshiba, K. Hayata, Finite-element analysis of quantum wells of arbitrary semiconductors with arbitrary potential profiles, IEEE J. Quantum Electron. 25 (1989) 889.
[7] P. Harrison, Quantum Wells, Wires, and Dots – Theoretical and Computational Physics, Wiley, New York, 2000.
[8] J.R. Chelikowsky, N. Troullier, Y. Saad, Finite-difference-pseudopotential method: electronic structure calculations without a basis, Phys. Rev. Lett. 72 (1994) 1240.
[9] S. Panda, B.K. Panda, S. Fung, Application of Fourier series methods for studying tunneling of electrons out of quantum wells in an electric field, J. Phys.: Condens. Matter 6 (1994) 887.
[10] Q.H. Liu, C. Cheng, H.Z. Massoud, The spectral grid method: a novel fast Schrödinger-equation solver for semiconductor nanodevice simulation, IEEE Trans. Comp. Aided Des. Integrated Circuits Syst. 23 (2004) 1200.
[11] K. Umashankar, A. Taflove, S.M. Rao, Electromagnetic scattering by arbitrary shaped three-dimensional homogeneous lossy dielectric objects, IEEE Trans. Antennas Propag. 34 (1986) 758.
[12] W.C. Chew, J.M. Jin, E. Michielssen, J. Song, Fast and Efficient Algorithms in Computational Electromagnetics, Artech House, 2001 (Chapter 11).
[13] X. Dong, Z. Liu, L. Carin, Volume and surface MLFMA formulation for dielectric targets in the presence of a half space, Radio Sci. 39 (2004).
[14] L. Greengard, V. Rokhlin, A fast algorithm for particle simulations, J. Comput. Phys. 73 (1987) 325.
[15] V. Rokhlin, Rapid solution of integral equations of scattering theory in two dimensions, J. Comput. Phys. 86 (1990) 414.
[16] V. Roklin, Diagonal forms of translation operators for the Helmholtz equation in three dimensions, Appl. Comput. Harm. Anal. 1 (1993) 82.
[17] R. Coifman, V. Rokhlin, S. Wandzura, The fast mutipole method for the wave equation: a pedestrian prescription, IEEE Antenna Propag. Mag. 35 (1993) 7.
[18] J.M. Song, C.C. Lu, W.C. Chew, Multilevel fast multipole algorithm for electromagnetic scattering by large complex objects, IEEE Trans. Antennas Propag. 45 (1997) 1488.
[19] N. Geng, A. Sullivan, L. Carin, Multilevel fast multipole for scattering from conducting targets above or embedded in a lossy half space, IEEE Trans. Geosci. Remote Sens. 38 (2000) 1561.
[20] R.F. Harrington, Field Computation by Moment Methods, Malabar, Robert E. Krieger Publishing Company, Florida, 1968.
[21] G.H. Golub, C.F. Van Loan, Matrix Computations, third ed., The John Hopkins University Press, 1996 (Chapter 17).
[22] S.M. Rao, D.R. Wilton, A.W. Glisson, Electromagnetic scattering from surfaces of arbitrary shape, IEEE Trans. Antennas Propag. 30 (1982) 409.
[23] Y. Saad, M. Schultz, GMRES: a generalized minimal residual algorithm for solving nonsymmetric linear systems, SIAM J. Sci. Statist. Comput. 7 (1986) 856.
[24] S. Koc, J.M. Song, W.C. Chew, Error analysis for the numerical evaluation of the diagonal forms of the scalar spherical addition theorem, SIAM J. Numer. Anal. 36 (1999) 906.
[25] L. Greengard, The Rapid Evaluation of Potential Fields in Particle Systems, MIT Press, Cambridge, 1988.
[26] L. Greengard, The numerical solution of the N-body problem, Comput. Phys. 4 (1990) 142.
[27] J.P. Boyd, Chebyshev and Fourier Spectral Methods, second ed., Dover, New York, 2001.